Cooperative Triple-Proton/Hydrogen Atom Relay in 7-Azaindole$(CH_3OH)_2$ in the Gas Phase: Remarkable Change in the Reaction Mechanism from Vibrational-Mode Specific to Statistical Fashion with Increasing Internal Energy

Kenji Sakota, Naomi Inoue, Yusuke Komoto, and Hiroshi Sekiya*

Department of Chemistry, Faculty of Sciences, and Department of Molecular Chemistry, Graduate School of Science. Kyushu University, 6-10-1 Hakozaki, Higashi-ku, Fukuoka 812-8581, Japan

Received: January 16, 2007; In Final Form: March 13, 2007

The 7-azaindole-methanol 1:2 cluster [7AI$(CH_3OH)_2$] undergoes excited-state triple-proton/hydrogen atom transfer (ESTPT/HT) along the hydrogen-bonded network in the gas phase. The measurements of the resonance-enhanced multiphoton ionization (REMPI) spectra of 7AI$(CH_3OH)_2$-d_n ($n = 0-3$), where subscript n indicates the number of deuterium, and the fluorescence excitation spectrum of 7AI$(CH_3OH)_2$-d_0 allowed us to investigate the ESTPT/HT dynamics. By comparing the intensity ratios of the vibronic bands between 7AI$(CH_3OH)_2$-d_0 and 7AI$(CH_3OH)_2$-d_3 in REMPI spectra, we obtained the lower limit of an acceleration factor (f_a^{low}) of 7AI$(CH_3OH)_2$-d_0, which is the ratio of the reaction rate for the excitation of a vibronic state to that of the zero-point state in S_1. The f_a^{low} values are 2.7 ± 0.83 and 4.0 ± 1.2 for an in-phase intermolecular stretching vibration (σ_1) and its overtone ($2\sigma_1$) observed at 181 cm^{-1} and 359 cm^{-1} in the excitation spectrum, respectively, while that of the vibration (ν_2/σ_1 or ν_3/σ_1) at 228 cm^{-1} is 1.1 ± 0.83. Thus, vibrational-mode-specific ESTPT/HT occurs in the low-energy region (600 cm^{-1}). The excitation of an intramolecular ring mode (ν_{intra}) of 7AI at 744 cm^{-1} substantially enhances the reaction rate ($f_a^{low} = 4.4 \pm 0.98$), but the increase of f_a^{low} is not prominent for the excitation of $\upsilon_{intra} + \sigma_1$ at 926 cm^{-1} ($f_a^{low} = 5.0 \pm 1.6$), although the σ_1 mode is excited. These results suggest that the ESTPT/HT reaction in 7AI$(CH_3OH)_2$-d_0 directly proceeds from the photoexcited states with the internal energy less than ~600 cm^{-1}, but it occurs from the isoenergetically vibrational-energy redistributed states when the internal energy is large. This shows a remarkable feature of ESTPT/HT in 7AI$(CH_3OH)_2$; the nature of the reaction mechanism changes from vibrational-mode specific to statistical fashion with increasing the internal energy. The hydrogen-bonded network in 7AI$(CH_3OH)_2$-d_0 is represented by a directed graph. This shows that ESTPT/HT is one of the simplest examples of cooperative phenomena.

Introduction

The proton and hydrogen atom transfer is one of the most basic chemical reactions and is important for the understanding of more complicated physical, chemical, and biological phenomena at the molecular level.[1] For example, the excited-state multiple-proton relay along the hydrogen-bonded network is a key reaction in revealing the fluorescence emitting mechanism of green fluorescent protein and its mutants,[2] which are widely used as fluorescence markers in the biological cells to clarify a function of a specific gene. The multiple-proton relay also plays an important role in a proton pump across a biomembrane of a cell through the proton wire, where the proton transport is achieved against a pH gradient in and outside the biomembrane.[3,4] In addition to the biological phenomena, the mechanism of the proton transport is a central issue in developing modern polymer electrolyte fuel cells and direct methanol fuel cells, where the multiple-proton relay in the water networks may proceed via Grotthuss mechanism.[5]

Spectroscopic investigations of the mechanism of the multiple-proton/hydrogen atom relay are useful in revealing characteristic features of the multiple proton/hydrogen atom relay at the molecular level. However, it is difficult to obtain quantitative information about the multiple proton/hydrogen atom relay by experimental studies of the molecular systems such as cells and fuel cells, because the solvent molecules, which do not directly participate in the proton relay along the hydrogen-bonded network, make the potential/free energy profiles quite complicated, although the solvent molecules that directly participate in the proton/hydrogen atom relay control the reaction at the molecular level. In addition, the analysis of the dynamics is difficult in the presence of thermal fluctuations of the hydrogen-bonded networks. Supersonically cooled hydrogen-bonded clusters are good model systems to investigate the dynamics of the multiple-proton/hydrogen atom relay at the molecular level, where the number of the solvent molecules can be controlled and the thermal fluctuation is insignificant.

One of recent topics in the excited-state dynamics of the heteroaromatic molecules and its hydrogen-bonded clusters is whether the proton transfers on the $\pi\pi^*$ surface or the hydrogen atom transfers through the $\pi\sigma^*$ surface occurs in the electronic excited state.[6−13] It is pointed out that the deactivation path from the electronic excited-state through the hydrogen atom transfer accompanied with two conical intersections of the $\pi\pi^*-\pi\sigma^*$ and $\pi\sigma^*-$ground state plays a crucial role for the photostability in the biological building blocks such as DNA bases.[12] In the gas phase, when the dissociative product via the $\pi\sigma^*$ state is detected, it is possible to confirm whether the proton or hydrogen atom transfer occurs by spectroscopic experiments.[6−11,13] For example, the occurrence of the hydrogen atom transfer has been confirmed in phenol$(NH_3)_n$ ($n = 0-5$), and quantum chemical

* Corresponding author. E-mail: hsekiscc@mbox.nc.kyushu-u.ac.jp.

10.1021/jp070359a CCC: $37.00
Published on Web 05/08/2007

SCHEME 1

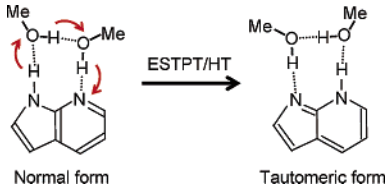

calculations of the excited-state potential energy surfaces of phenol$(NH_3)_3$ are consistent with the experimental results.[6−11,13] Furthermore, the mode-specific hydrogen atom transfer through the $\pi\sigma^*$ surface has been observed in phenol$(NH_3)_1$.[14] However, it is generally difficult to determine whether the proton or hydrogen atom relay occurs from spectroscopic experiments when the proton/hydrogen atom relay along the hydrogen-bonded network is not dissociative.

In the last few decades, detailed mechanism of the single- and double-proton transfer was clarified by spectroscopic and theoretical studies.[15−57] The mechanisms of the single- and double-proton transfer in the molecules and hydrogen-bonded clusters studied so far provide insights into the multiple-proton/hydrogen atom relay in the hydrogen-bonded network. For example, it was revealed that both the intra- and intermolecular proton tunneling should be described by the multidimensional potential energy surface, i.e., the moving proton(s) couples with the motions of the heavy atoms. In the hydrogen-bonded clusters such as 7-hydroxyquinoline(7-HQ)$(CH_3OH)_3$ and 7-HQ$(NH_3)_3$, the proton and/or hydrogen atom relay occurs along the hydrogen-bonded solvent wire (i.e., one-dimensional hydrogen-bonded network) by the photoexcitation of the clusters in the gas phase.[58−63] The influence of the motion of the solvent molecules to ESHT in 7-HQ$(NH_3)_3$ was investigated by Leutwyler's group.[62] However, it has not been well understood how the motions of the solvent molecules (i.e., the heavy atom motions) influence the proton and/or hydrogen atom relay dynamics.

The excited-state double-proton transfer (ESDPT) was observed for 7-azaindole dimer ($7AI_2$) and the substituted $7AI_2$. The mechanism of ESDPT in $7AI_2$ was studied in details by spectroscopic experiments in the gas and condensed phase, together with theoretical calculations.[21−57] On the other hand, in the condensed phase, ESDPT was observed for 7AI(alcohol)$_1$ (alcohols used are methanol, ethanol, buthanol, etc.) and 7AI$(H_2O)_1$.[23,64−69] A two-step model of ESDPT was proposed for 7AI(alcohol)$_1$ and 7AI$(H_2O)_1$. In the two step model, the photoexcited 7AI(alcohol)$_1$ and 7AI$(H_2O)_1$ clusters undergo the solvent reorganization into the optimal precursor followed by ESDPT. This model is widely accepted as the mechanism of ESDPT in 7AI(alcohol)$_1$ and 7AI$(H_2O)_1$ in the condensed phase. In addition, on the basis of the analysis of the viscosity-dependent ESDPT rate and its kinetic isotope effect (KIE), it was suggested that the solvent fluctuation including the motions of the heavy atoms (i.e., N and O atoms) of 7AI and water or alcohols assists ESDPT.[69] It was pointed out that the low-frequency vibrations in protein (i.e., the heavy atom motions) assist the hydrogen tunneling in the catalytic reaction in the enzyme at around the room temperature.[69−71] Therefore, the investigation of the role of the heavy atom motions in multiple-proton/hydrogen atom relay in the hydrogen-bonded clusters may provide insight into the mechanism in the catalytic reactions of enzymes.

Very recently, we reported the excited-state triple proton/hydrogen atom transfer (ESTPT/HT) in 7AI$(CH_3OH)_2$ in the gas phase (Scheme 1).[70] It was shown that the in-phase intermolecular stretching vibration, which is the cooperative motion of the whole hydrogen-bonded network, enhances ESTPT/HT in 7AI$(CH_3OH)_2$. In contrast, no evidence for the formation of the tautomeric forms has been obtained for 7AI$(CH_3OH)_n$ ($n = 1, 3$) from the dispersed fluorescence spectroscopy. In the present work, we report new aspects of the ESTPT/HT reaction in 7AI$(CH_3OH)_2$. We have determined the relative reaction rates for vibronic states in the S_1 state by analyzing the resonance-enhanced multiphoton ionization (REMPI) spectra of the isotopomers. The most prominent finding is that the nature of the mechanism of ESTPT/HT in the S_1 state drastically changes from vibrational-mode specific in the low-energy region to statistical fashion in the high-energy region. We briefly discuss ESTPT/HT as a simple model system to investigate the cooperative phenomena.

Experimental

The experimental setup was described elsewhere.[49−52,70] The sample introduced in a stainless tube was heated to 353 K by a coiled heater and expanded into the vacuum chamber with Ne as a carrier gas. The backing pressure was 2.5 atm. The carrier gas passes through a reservoir containing undeuterated and/or deuterated methanol. A pulsed valve (General Valve, series 9, 0.5 mm diameter) was operated at 10 Hz. The REMPI spectra were measured with a differentially pumped linear time-of-flight mass spectrometer with a mass gate. For the REMPI experiments, a frequency-doubled dye-laser (Sirah Cobra stretch) pumped by a second harmonic of a Nd^{3+}:YAG laser (Spectra Physics GCR 230) was used. The UV−UV hole-burning spectra were measured by using a frequency-doubled dye-laser (Spectra Physics PDL-3 and Inrad Autotracker III) pumped by a second harmonic of the Nd^{3+}:YAG laser (Spectra Physics GCR 150) as a pump laser. The fluorescence excitation (FE) spectra were measured by using a frequency-doubled dye-laser (Sirah Cobra stretch) pumped by a second harmonic of the Nd^{3+}:YAG laser (Spectra Physics GCR 230), and only UV or visible emission was detected by a photomultiplier (Hamamatsu R955) with Toshiba UV35+UV-D33S glass filters for UV emission and a Toshiba Y51 glass filter for visible emission. REMPI and FE spectra were calibrated against the laser powers. 7AI, undeuterated, and deuterated methanol were purchased from TCI, Wako, and Aldrich Co. Ltd., respectively. They were used without further purification.

Quantum chemical calculations at the B3LYP level were carried out for the S_0 and D_0 state with the 6-31++G** basis sets for the hydrogen-bonded hydrogen atoms, all nitrogen and oxygen atoms, and with the 6-31G* basis sets for the other atoms. The stable structures were obtained for the S_1 state by CIS/6-31++G**/6-31G* calculations, while the energies of each structure were obtained by TDB3LYP/6-31++G**/6-31G* calculations. The harmonic vibrational frequencies are calculated by CIS/6-31++G**/6-31G* calculations. All calculations were performed by using a GAUSSIAN 03 program package.

Results

Figure 1a,b shows the UV−UV hole-burning and REMPI spectra of 7AI$(CH_3OH)_2$ in the S_1-S_0 ($\pi\pi^*$) region. These spectra clearly show that only a single isomer is detected under our experimental conditions. In the case of 7AI$(H_2O)_n$ ($n = 1-3$), evidence of cyclic structures, where two water molecules bridge an NH group and a heteroaromatic N atom of 7AI, is obtained by the rotationally resolved FE spectra and the IR-dip spectra.[37,71] The vibronic structures of S_1-S_0 electronic spectra

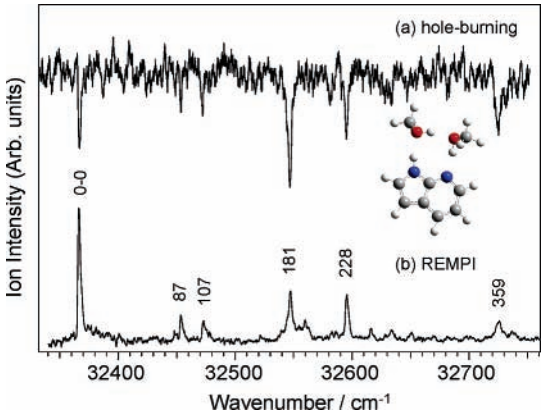

Figure 1. (a) UV−UV hole-burning and (b) REMPI spectra of 7AI-$(CH_3OH)_2$. The 0−0 transition is observed at 32367 cm^{-1}. The relative wave numbers ($\nu(0-0) - \nu$) of prominent vibronic bands are indicated in the figure.

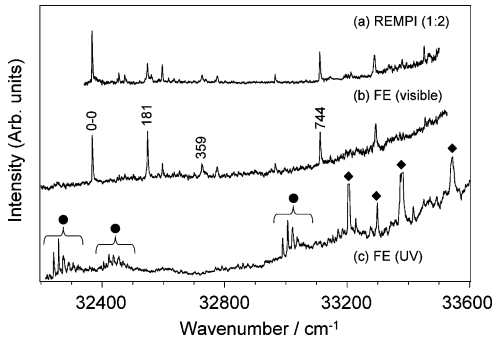

Figure 2. (a) REMPI spectrum of 7AI$(CH_3OH)_2$. FE spectra measured by detecting (b) visible fluorescence and (c) UV fluorescence. Closed circles and closed squares correspond to the vibronic bands of 7AI-$(CH_3OH)_3$ and 7AI$(CH_3OH)_1$, respectively. The transitions of the vibronic bands of 7AI$(CH_3OH)_1$ are saturated.

of 7AI$(H_2O)_2$ and 7AI$(CH_3OH)_2$ in the region of the intermolecular vibrations are quite similar.[70,72] We carried out quantum chemical calculations at the CIS/6-31+G**/6-31G* level for S_1 and B3LYP/6-31+G**/6-31G* levels for S_0; The stable structure of 7AI$(CH_3OH)_2$ is similar to that of 7AI$(H_2O)_2$.[70] These results suggest that 7AI$(CH_3OH)_2$ has a cyclic structure, where two methanol molecules bridge an NH group and a heteroaromatic N atom of 7AI. We have already reported that ESTPT and/or ESHT occurs in 7AI$(CH_3OH)_2$. Hereafter we use an abbreviation ESTPT/HT, since it is difficult to distinguish the two mechanisms at this stage.[70] The structure of 7AI$(CH_3OH)_2$ obtained by CIS/6-31++G**/6-31G* calculation is inserted in Figure 1.

Figure 2a−c shows the REMPI spectrum of 7AI$(CH_3OH)_2$ and FE spectra obtained by detecting visible and UV emission, respectively. It is worth noting that visible fluorescence is detected only from the tautomeric form of 7AI$(CH_3OH)_2$, while all vibronic bands in Figure 2b also appear in Figure 2a. On the other hand, the vibronic bands of 7AI$(CH_3OH)_1$ and 7AI-$(CH_3OH)_3$ in Figure 2c are not detected in Figure 2b. These results clearly indicate that the visible fluorescence from the tautomeric form originates from ESTPT/HT in 7AI$(CH_3OH)_2$ in this energy region. The relative intensity of a vibronic band at $\nu(0-0) + 181$ cm^{-1} to the 0−0 band is prominently stronger in the FE spectrum than that in the REMPI spectrum. Based on the normal mode calculation, the band at $\nu(0-0) + 181$ cm^{-1} was assigned to an intermolecular stretching mode (σ_1), which exhibits in-phase cooperative motion of the whole hydrogen-bonded network.[70]

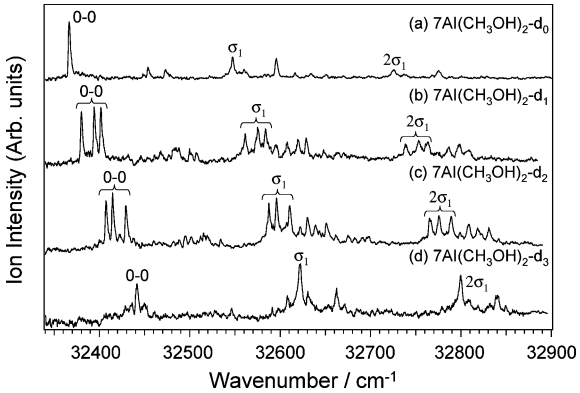

Figure 3. REMPI spectra of (a) 7AI$(CH_3OH)_2$-d_0, (b) 7AI$(CH_3OH)_2$-d_1, (c) 7AI$(CH_3OH)_2$-d_2, and (d) 7AI$(CH_3OH)_2$-d_3. The 0−0 transitions of 7AI$(CH_3OH)_2$-d_0, 7AI(CH_3OH)2-d_1, 7AI$(CH_3OH)_2$-d_2, and 7AI$(CH_3OH)_2$-d_3 are observed at 32367, 32381, 32407, and 32442 cm^{-1}, respectively. Three strong origins are observed in the spectra of 7AI-$(CH_3OH)_2$-d_1 and 7AI$(CH_3OH)_2$-d_2 (see Supporting information). Here, we show only the 0−0 bands detected at the lowest wavenumber. Notations σ_1 and $2\sigma_1$ are the fundamentals and overtones of the in-phase intermolecular stretching vibration, respectively. The displacements of the atoms in the σ_1 mode are shown in Figure 5.

Figure 3 shows the REMPI spectra of the deuterated 7AI-$(CH_3OH)_2$-d_n ($n = 0-3$), where subscript n indicates the number of deuterium. Figure 3a is the same REMPI spectrum as Figure 1a. Panels b and c of Figure 3 display the REMPI spectra of 7AI$(CH_3OH)_2$-d_1 and 7AI$(CH_3OH)_2$-d_2, respectively. The 0−0 bands of 7AI$(CH_3OH)_2$-d_1 and 7AI$(CH_3OH)_2$-d_2 are observed at 32381and 32407 cm^{-1}, which are 14 and 40 cm^{-1} blue-shifted from that of 7AI$(CH_3OH)_2$-d_0, respectively. The vibronic bands observed in Figure 3b,c split into three components. In 7AI-$(CH_3OH)_2$-d_0, the NH hydrogen in 7AI and the OH hydrogen in the two CH_3OH molecules may be preferentially deuterated. Therefore, there are three isotopomers for both 7AI$(CH_3OH)_2$-d_1 and 7AI$(CH_3OH)_2$-d_2, whose zero-point energies are different one another. The assignments for the three isotopomers of 7AI-$(CH_3OH)_2$-d_1 and 7AI$(CH_3OH)_2$-d_2 are described in detail in Supporting Information. The three isotopomers of 7AI$(CH_3OH)_2$-d_1 and 7AI$(CH_3OH)_2$-d_2 show very similar vibronic patterns, suggesting that the effect of deuteration on the vibrational distribution is insignificant.

Figure 3d shows the REMPI spectrum of 7AI(CH_3OH_2)-d_3. The 0−0 band of 7AI$(CH_3OH)_2$-d_3 at 32442 cm^{-1} is 75 cm^{-1} blue-shifted from that of 7AI$(CH_3OH)_2$-d_0. Both strong and very weak vibronic bands are detected in Figure 3d. The strong vibronic bands in Figure 3d are assigned to 7AI$(CH_3OH)_2$-d_3, where the NH hydrogen in 7AI and the OH hydrogen in the two CH_3OH molecules are deuterated. The weak vibronic bands around the strong bands are assigned to another isotopomers of 7AI$(CH_3OH)_2$-d_3, where the CH hydrogen(s) may be deuterated. The relative intensities of the vibronic bands to each 0−0 band are very different in Figure 3a−d, suggesting that the rate of ESTPT/HT that generates the tautomeric forms substantially depends on the number of the deuterated atoms, i.e., ESTPT/HT in 7AI$(CH_3OH)_2$ exhibits remarkable KIE.

Figure 4a,b displays the REMPI spectra of 7AI$(CH_3OH)_2$-d_0 and 7AI$(CH_3OH)_2$-d_3 including vibronic bands at higher energy region than those in Figure 3. The vibronic bands observed at $\nu(0-0) + 744$ and $\nu(0-0) + 1088$ cm^{-1} of 7AI$(CH_3OH)_2$-d_0 are assigned to intramolecular vibrational modes from the comparison of the wavenumbers of the observed vibronic bands with those obtained by the ab initio calculation at the CIS/6-31++G**/6-31G* level. The corresponding vibrational modes in 7AI$(CH_3OH)_2$-d_3 are detected at $\nu(0-0) + 744$ and $\nu(0-0)$

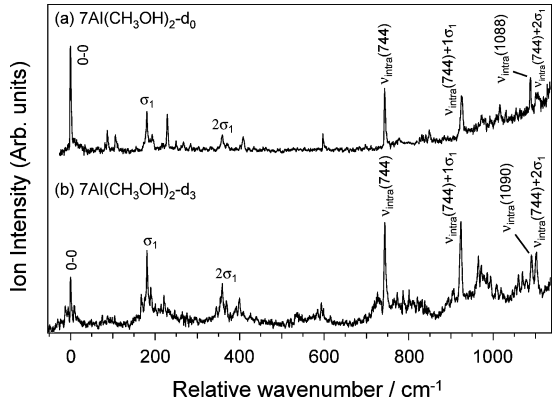

Figure 4. REMPI spectra of (a) $7AI(CH_3OH)_2$-d_0 and (b) $7AI(CH_3OH)_2$-d_3. The abscissa is the relative wavenumber from the 0−0 bands in the two spectra. The assignments of the main vibronic bands are indicated in the figure. The displacements of the atoms in the vibrations σ_1, $\nu_{intra}(744)$, and $\nu_{intra}(1088)$ are shown in Figure 5.

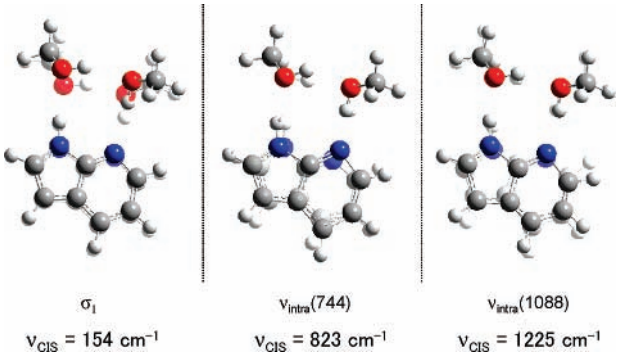

Figure 5. Normal modes of $7AI(CH_3OH)_2$-d_0 calculated at the CIS/6-31++G**/6-31G* level of theory. ν_{CIS} indicates the calculated wavenumber (not scaled). The displacements of the atoms in $\nu_{intra}(744)$ and $\nu_{intra}(1088)$ are mainly localized on the 7AI ring.

+ 1090 cm^{-1}, respectively. The displacements of the atoms in these vibrational modes are illustrated in Figure 5. We also observed a combination band $\nu_{intra}(744) + 1\sigma_1$ at $\nu(0-0)$ + 925 cm^{-1} in the spectrum of $7AI(CH_3OH)_2$-d_0, and those of $\nu_{intra}(744) + 1\sigma_1$ and $\nu_{intra}(744) + 2\sigma_1$ at $\nu(0-0)$ + 923 and $\nu(0-0)$ + 1102 cm^{-1} in the spectrum of $7AI(CH_3OH)_2$-d_3, respectively. The combination band $\nu_{intra}(744) + 2\sigma_1$ of $7AI(CH_3OH)_2$-d_0 is too weak to determine the accurate position.

Discussion

A. Difference of the Ionization Cross Sections between Normal and Tautomeric Forms. It is clear from Figure 2 that the relative intensity of $1\sigma_1$ (181 cm^{-1}) to the 0−0 band in the FE spectrum of $7AI(CH_3OH)_2$ is very different from that in the REMPI spectrum. In $7AI_2$, the ionization cross section from the S_1 state of the tautomer is much smaller than that from the normal form. By analogy, it is reasonable to assume that the ionization cross section in the tautomeric form of $7AI(CH_3OH)_2$ is smaller than that in the normal form of $7AI(CH_3OH)_2$. Therefore, the remarkable difference in the relative intensities between the FE and REMPI spectra in Figure 2 is due to the acceleration of ESTPT/HT when the vibronic bands containing the σ_1 mode are excited.

In order to confirm the validity of the assumption described above, we carried out DFT calculations at the B3LYP/6-31++G**/6-31G* level for S_0 and D_0 and at the TDB3LYP/6-31++G**/6-31G* level for S_1. The results are summarized in Figure 6. The calculated $S_1-S_0(\pi\pi^*)$ transition energy of

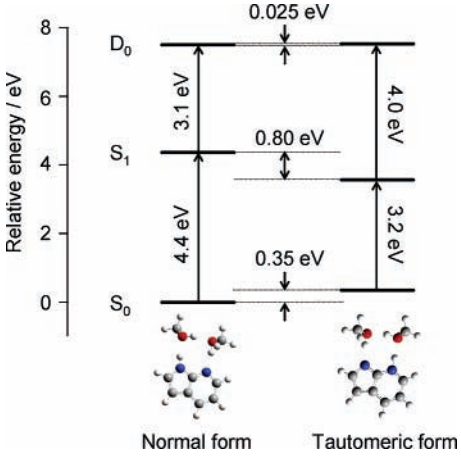

Figure 6. Energy diagram for $7AI(CH_3OH)_2$-d_0. The energies of S_0 and D_0 were calculated at the B3LYP/6-31++G**/6-31G* level, while that of S_1 was calculated at the TDB3LYP/6-31++G**/6-31G* level for stable structures obtained by the calculations at the CIS/6-31++G**/6-31G* level. In the D_0 state, the energy of the normal form of $7AI(CH_3OH)_2$ is stable by 0.025 eV, as compared with the energy of the tautomeric form.

the normal form of $7AI(CH_3OH)_2$ is larger than the experimental one. However, the relative energies in the same electronic states may be reliable since the errors originated from the electronic correlations may be similar in the same electronic states; therefore, the total errors are canceled to a certain extent. The relative energies of the normal and tautomeric forms of $7AI(CH_3OH)_2$ strongly depend on the electronic states. The normal form of $7AI(CH_3OH)_2$ is more stable than the tautomeric form in S_0. However, the relative energy between the normal and tautomeric forms is reversed in S_1; the energy of the tautomeric form is substantially lower than that of the normal form. The calculated energies are consistent with the observation of largely red-shifted fluorescence from the tautomer.

The calculated energies of the D_0 state of the normal and tautomeric forms of $7AI(CH_3OH)_2$ are similar, although the relative energies of S_0 and S_1 are very different. As a result, the $D_0 \leftarrow S_1$ transition energy of the tautomeric form is much larger than that of the normal form. It should be noted that the ionization of the tautomeric form of $7AI(CH_3OH)_2$ occurs from the S_1 vibronic states with large vibrational quantum numbers, because the energy difference between the normal and tautomeric forms in S_1 is very large. The Δv propensities for the $D_0 \leftarrow S_1$ transitions of the normal and tautomeric forms may be roughly similar, because electronic characters of both the normal and tautomeric forms in S_1 and D_0 are similar. Thus, the effective excess energy of the tautomeric form of D_0 is much smaller than that of the normal form. Therefore, the ionization efficiency from S_1 of the tautomeric form is much smaller than that of the normal form of $7AI(CH_3OH)_2$. These arguments are consistent with the assumption that the ionization cross section from S_1 of the tautomeric form is much smaller than that of the normal form.

B. Analysis of Vibrational Mode-Specific ESTPT/HT. In the previous communication, we showed that the vibrational-mode specific ESTPT/HT occurs in $7AI(CH_3OH)_2$.[70] However, the differences in the ESTPT/HT rates between vibronic states have not been quantitatively analyzed. The relative ESTPT/HT rates for some vibronic bands have been obtained by measuring the REMPI spectra of isotopomers.

Figure 3 displays the REMPI spectra of the deuterated $7AI(CH_3OH)_2$ clusters. The relative intensities of the in-phase intermolecular stretching bands (σ_1) to the 0−0 bands are

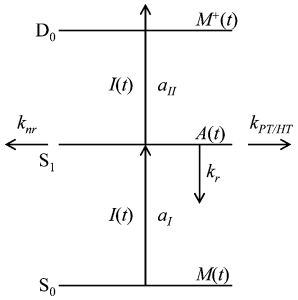

Figure 7. Schematic energy level diagram of the normal form of 7AI-$(CH_3OH)_2$. $M(t)$, $A(t)$, and $M^+(t)$ indicate the populations of the normal 7AI$(CH_3OH)_2$ in S_0, S_1, and D_0, respectively. a_I and a_{II} indicate the absorption cross sections for the $S_1 \leftarrow S_0$ and $D_0 \leftarrow S_1$ transitions, respectively. $k_{PT/HT}$, k_r, and k_{nr} indicate the rate constants for ESTPT/HT, the radiative decay from S_1 to S_0, and the nonradiative decay from S_1, respectively. $I(t)$ indicates the laser intensity.

different between the spectra in Figure 3a−d. In particular, the intensity distribution of vibronic bands in 7AI$(CH_3OH)_2$-d_3 is very different from that in 7AI$(CH_3OH)_2$-d_0. In 7AI$(CH_3OH)_2$-d_0, the excitation of vibronic bands containing the σ_1 mode promotes ESTPT/HT relative to the zero-point level, whereas ν_2/σ_3 (or ν_3/σ_3) has little effect on ESTPT/HT, where ν_2/σ_3 (or ν_3/σ_3) is the OH...O intermolecular stretch mode (σ_3) of the methanol molecules mixed with an intramolecular out-of-plane modes (ν_2 or ν_3).[70] Therefore, the vibronic pattern in the REMPI spectrum of 7AI$(CH_3OH)_2$-d_0 must be very different from that predicted from the Franck−Condon distribution when the vibrational-mode specific ESTPT/HT reaction occurs; i.e., the intensity distribution in the REMPI spectrum may significantly depend on the relative rate for ESTPT/HT to the ionization rate from S_1 state of the normal form. On the basis of the ab initio calculations in ref 70, there are potential energy barriers along the ESTPT and ESTHT reaction paths. Therefore, ESTPT/HT may occur via the tunneling mechanism. In 7AI$(CH_3OH)_2$, three hydrogen must transfer to generate the tautomeric form. Hence, KIE is predicted to be large, and the radiative and nonradiative transitions from S_1 become much faster than the ESTPT/HT rate in 7AI$(CH_3OH)_2$-d_3. It is reasonable to consider that the vibrational intensity distribution in 7AI$(CH_3OH)_2$-d_3 reflects the Franck−Condon distribution. We note that the relative intensities of the σ_1 bands to the 0−0 bands gradually increases on going from 7AI$(CH_3OH)_2$-d_0 to 7AI$(CH_3OH)_2$-d_3. On the basis of the assumption that the ionization cross section from $S_1(\upsilon = 0, \sigma_1)$ to D_0 does not depend on the degree of deuteration, this implies that the ESTPT/HT rate gradually reduces with increasing the number of deuterated atoms in comparison with the ionization rate. This observation is consistent with the tunneling mechanism in ESTPT/HT.

In order to analyze the vibrational mode-specific ESTPT/HT quantitatively, a kinetic model illustrated in Figure 7 is employed. The rate equations representing the numbers of clusters in each electronic state are given by

$$\frac{dM(t)}{dt} = -a_I I(t) M(t) \tag{1}$$

$$\frac{dA(t)}{dt} = a_I I(t) M(t) - a_{II} I(t) A(t) - (k_r + k_{nr} + k_{PT/HT}) A(t) \tag{2}$$

$$\frac{dM^+(t)}{dt} = a_{II} I(t) A(t) \tag{3}$$

where $M(t)$, $A(t)$, and $M^+(t)$ are the populations of clusters in S_0, S_1, and D_0, respectively, while a_I and a_{II} are the $S_1 \leftarrow S_0$ and $D_0 \leftarrow S_1$ absorption cross sections, respectively. $I(t)$ is the laser intensity, while k_r, k_{nr}, and $k_{PT/HT}$ are the radiative decay constant for the $S_1 \rightarrow S_0$ transition, the nonradiative decay constant, and the ESTPT/HT rate constant, respectively.

In the condensed phase, the occurrence of ESPT (excited-state proton transfer) was reported for 7AI$(CH_3OH)_1$. The time constant of ESPT was measured to be ∼100 ps.[67,69] The experimental conditions are different between the gas phase and the condensed phase. However, if we assume that the time constant of ESPT in the condensed phase is close to that of ESTPT/HT in the gas phase, $(k_{PT/HT})^{-1}$ may be ∼100 ps. This value suggests that ESTPT/HT in 7AI$(CH_3OH)_2$-d_0 is a fairly fast process. Therefore, k_r and k_{nr} can be ignored as compared with the $k_{PT/HT}$ value. For simplicity, we assume that the laser intensity does not depend on time, although the laser pulse used has a time-dependent intensity profile. We also assume the steady-state condition for S_1. Under these assumptions we obtained the following relation with eqs 1−3:

$$\frac{k_{PT/HT}(\upsilon) + a_{II} I}{k_{PT/HT}(0-0) + a_{II} I} \approx \frac{M^+(0-0)}{M^+(\upsilon)} \frac{a_I(\upsilon)}{a_I(0-0)} \tag{4}$$

where $k_{PT/HT}(0-0)$ and $k_{PT/HT}(\upsilon)$ are the ESTPT/HT rates for the excitation of the 0−0 state and the vibronic state of 7AI-$(CH_3OH)_2$-d_0, respectively. $M^+(0-0)/M^+(\upsilon)$ indicates the intensity ratio of the 0−0 band to a vibronic band in the spectrum of 7AI$(CH_3OH)_2$-d_0. $a_I(\upsilon)/a_I(0-0)$ corresponds to the ratio of the Franck−Condon factor of the $S_1 \leftarrow S_0$ $(\upsilon-0)$ transition to the 0−0 transition of 7AI$(CH_3OH)_2$-d_0. In 7AI$(CH_3OH)_2$-d_3, the ESTPT/HT rate may be much smaller than the radiative and nonradiative rates. Therefore, the vibronic distribution in the REMPI spectrum of 7AI$(CH_3OH)_2$-d_3 should be very similar to the Franck−Condon distribution. Thus, we can obtain $a_I(\upsilon)/a_I(0-0)$ for 7AI$(CH_3OH)_2$-d_0 by using the intensity distribution in the REMPI spectrum of 7AI$(CH_3OH)_2$-d_3 as a reference.

In the left-hand side of eq 4, a term $a_{II}I$ exists in both the numerator and denominator, which makes the analysis of eq 4 difficult. However, under the condition of $a_{II}I \ll k_{PT/HT}$ the following equation is derived:

$$\frac{k_{PT/HT}(\upsilon)}{k_{PT/HT}(0-0)} \approx \frac{M^+(0-0)}{M^+(\upsilon)} \frac{a_I(\upsilon)}{a_I(0-0)} \tag{5}$$

In eq 5, the term in the left-hand side corresponds to the ratio of the ESTPT/HT rate constant of the vibronic state ν to the zero-point state. The condition $a_{II}I \ll k_{PT}$ is not necessarily satisfied, thus the following inequality 6 is derived, because the left-hand side of the eq 4 is smaller than that of the eq 5:

$$\frac{k_{PT/HT}(\upsilon)}{k_{PT/HT}(0-0)} \geq \frac{M^+(0-0)}{M^+(\upsilon)} \frac{a_I(\upsilon)}{a_I(0-0)} \tag{6}$$

Hence, we can estimate the lower limit of the relative rate constant of the vibronic state to the 0−0 state from eq 6. We define $f_a \equiv k_{PT/HT}(\upsilon)/k_{PT/HT}(0-0)$ as an acceleration factor. Several values of the lower limit of the accelerating factor, f_a^{low}, are plotted in Figure 8, together with the REMPI spectrum of 7AI$(CH_3OH)_2$-d_0. Table 1 summarizes the f_a^{low} values. The f_a^{low} value of $1\sigma_1$ is 2.7 ± 0.83, while that of the ν_2/σ_3 (or ν_3/σ_3) state at 228 cm^{-1} is 1.1 ± 0.83. Although the energy difference between the $1\sigma_1$ and ν_2/σ_3 (or ν_3/σ_3) states is only 48 cm^{-1}, the f_a^{low} values of $1\sigma_1$ (2.7 ± 0.83) and ν_2/σ_3 (or ν_3/σ_3)(f_a^{low}= 1.1 ± 0.83) are explicitly different. The f_a^{low} value of the $2\sigma_1$ state is 4.0 ± 1.2, which shows further enhancement of the ESTPT/

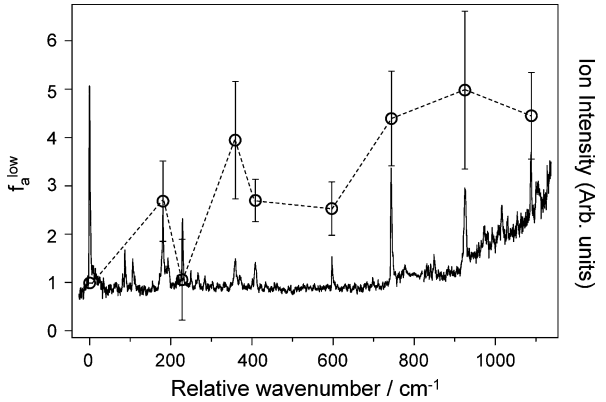

Figure 8. The lower limit of the acceleration factors (f_a^{low}) of vibronic bands in the REMPI spectrum of 7AI$(CH_3OH)_2$ obtained with eq 6 are plotted against the relative wavenumber.

TABLE 1: f_a^{low} Values and Assignment for Vibronic Bands of 7AI$(CH_3OH)_2$

relative wavenumber (cm^{-1})	f_a^{low} [a]	assignment
0	1	0−0
181	2.7 ± 0.83	$1\sigma_1$
228	1.1 ± 0.83	ν_2/σ_3 or ν_3/σ_3
359	4.0 ± 1.2	$2\sigma_1$
409	2.7 ± 0.44	ν_2/σ_3 (or ν_3/σ_3) + $1\sigma_1$
598	2.5 ± 0.55	$\nu_{intra}(598)$
744	4.4 ± 0.98	$\nu_{intra}(744)$
925	5.0 ± 1.6	$\nu_{intra}(744) + 1\sigma_1$
1088	4.5 ± 0.89	$\nu_{intra}(1088)$

[a] f_a^{low} is the lower limit of the acceleration factor. The definition of the acceleration factor is given in eq 6.

HT rate by exciting two quanta of the σ_1 mode. A vibronic band at 409 cm^{-1} is assigned to the combination band of the ν_2/σ_3 (or ν_3/σ_3) and $1\sigma_1$ modes. The f_a^{low} value of this state is 2.7 ± 0.44, which is almost the same as the value of the $1\sigma_1$ state. A very similar f_a^{low} value of the ν_2/σ_3 (or ν_3/σ_3) + $1\sigma_1$ state to the $1\sigma_1$ state suggests that the excitation of $1\sigma_1$ in the combination modes is responsible for the enhancement of the f_a^{low} value.

C. Appearance of Statistical Nature in ESTPT/HT with Increasing the Internal Energy. In Figure 8, we show the acceleration factors (f_a^{low}) for an intramolecular vibrational mode at 744 cm^{-1} ($\nu_{intra}(744)$) and its combination band at 925 cm^{-1} ($\nu_{intra}(744) + 1\sigma_1$). The f_a^{low} value for the excitation of one quantum of $\nu_{intra}(744)$ is 4.4 ± 0.98, which is much larger than that for $1\sigma_1$. On the other hand, the f_a^{low} value of $\nu_{intra}(744)$ + $1\sigma_1$ is 5.0 ± 1.6. The f_a^{low} value of $\nu_{intra}(744) + 1\sigma_1$ is only 1.1 times larger than that for $\nu_{intra}(744)$, although $\nu_{intra}(744) + 1\sigma_1$ contains the σ_1 mode. It should be noted that the acceleration factor of $\nu_{intra}(1088)$ is 4.5 ± 0.86, which is also similar to those of $\nu_{intra}(744)$ and $\nu_{intra}(744) + 1\sigma_1$.

It is surprising from the view point of the vibrational-mode specific reaction that the $\nu_{intra}(744)$ mode promotes the ESTPT/HT reaction, because the displacement of the $\nu_{intra}(744)$ mode contains a little component along the ESTPT/HT coordinate. Similarly, only a little increase of the f_a^{low} value of $\nu_{intra}(744)$ + $1\sigma_1$ as compared with that of $\nu_{intra}(744)$ cannot be well explained by the vibrational-mode specific reaction, since $\nu_{intra}(744) + 1\sigma_1$ involves the displacements along the ESTPT/HT reaction coordinate. These observations indicate the disappearance of the vibrational-mode selectivity in ESTPT/HT. This new feature of ESTPT/HT can be elucidated by considering the vibrational-energy dissipation paths from the initially excited states. When $\nu_{intra}(744)$ is excited, the intracluster vibrational energy redistribution (IVR) may occur, and ESTPT/HT does not occur directly from the $\nu_{intra}(744)$ state, but from the isoenergetically vibrational energy redistributed states that partially contain the σ_1 mode. Therefore, when the $\nu_{intra}(744)$ state is photoexcited, the σ_1 component in the isoenergetically redistributed states contribute to the acceleration of ESTPT/HT. Similarly, when the $\nu_{intra}(744) + 1\sigma_1$ state is photoexcited, IVR may proceed from the $\nu_{intra}(744) + 1\sigma_1$ state. The memory of the initially excited state ($\nu_{intra}(744) + 1\sigma_1$) is erased due to IVR, so that the vibrational-mode specificity disappears. The redistributed states from the $\nu_{intra}(744) + 1\sigma_1$ state should contain the σ_1 component. Therefore, ESTPT/HT accelerates by exciting $\nu_{intra}(744) + 1\sigma_1$. The f_a^{low} value of $\nu_{intra}(1088)$ is similar to those of $\nu_{intra}(744)$ and $\nu_{intra}(744) + 1\sigma_1$. This may be also due to IVR.

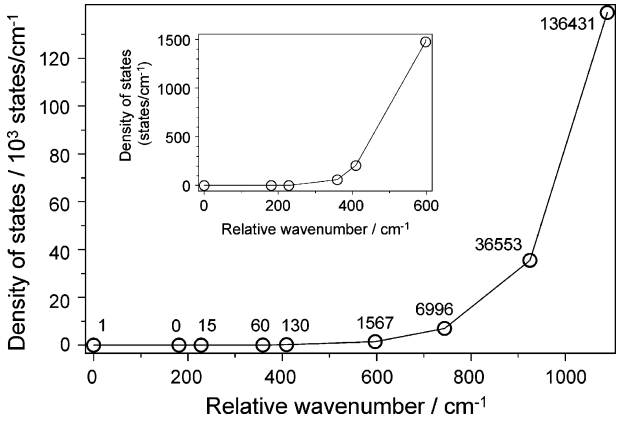

Figure 9. The density of states of each vibronic state of 7AI$(CH_3OH)_2$ are calculated by the Beyer−Swinehart direct counting algorism. The harmonic vibrational wavenumbers are obtained by calculation at the CIS/6-31++G**/6-31G* level. The accurate density of states of each vibronic state is indicated in the figure. The inserted figure shows an expansion of the density of states in the $\Delta\nu = 0-600$ cm^{-1} region. The solid line connecting each point is only to guide the eye.

The relative rate constants for ESTPT/HT and IVR are quite important to determine the vibrational mode-specific nature or the statistical nature in ESTPT/HT. As is discussed above, the time constant for ESTPT/HT in the gas phase may be close to the ESPT time constant in the condensed phase (∼100 ps). The observation of the similar acceleration factors for the $\nu_{intra}(744)$, $\nu_{intra}(744) + 1\sigma_1$, and $\nu_{intra}(1088)$ states suggests that IVR proceeds faster than ESTPT/HT. Therefore, in the energy region where the statistical nature is observed in ESTPT/HT, IVR may proceed faster than the order of 100 ps, although the possibility that IVR competes with ESTPT/HT cannot be excluded completely.

At the present stage, it is difficult to estimate the rate for IVR in 7AI$(CH_3OH)_2$. However, it is well-known that the IVR rate is roughly proportional to the density of states at the given internal energy (i.e., Fermi's golden rule), although it has been proposed that the doorway state(s) plays an important role in the IVR dynamics in some cases (i.e., Tier model).[73] In order to estimate the tendency of changing the IVR rate with the internal energy, we calculated the density of states by the Beyer−Swinehart direct counting algorism.[74] Figure 9 displays the calculated density of states. The vibrational frequencies obtained by CIS/6-31++G**/6-31G* calculation were used to estimate the density of states. Although the calculated density of states should contain some errors originating from the ignorance of the anharmonic effects and the inaccuracy of the calculated vibrational frequencies, we can infer the change of the IVR rate with the internal energy from Figure 9. Up to the

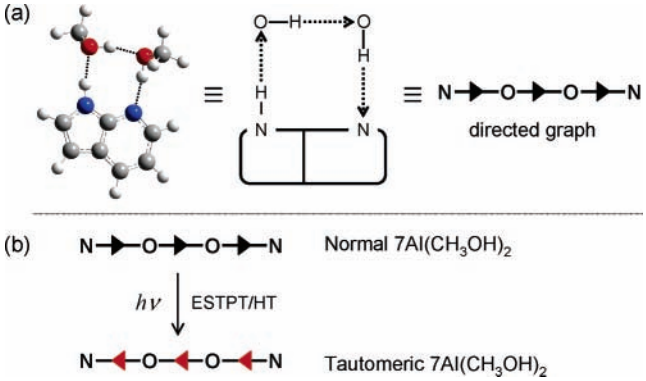

Figure 10. (a) Schematic representation of the directed graph. The directions of the arrows correspond to that of each hydrogen bond. The hydrogen-bonded network in $7AI(CH_3OH)_2$ can be illustrated as a one-dimensional hydrogen-bond network. (b) Directed graphs of the normal and tautomeric forms of $7AI(CH_3OH)_2$. Upon photoexcitation the normal form undergoes ESTPT/HT reaction, leading to the reversed directions of the hydrogen bonds over whole hydrogen-bonded network in the tautomeric form.

energy of the ν_2/σ_3 (or ν_3/σ_3) + $1\sigma_1$ state, the vibrational mode-specific nature was observed in ESTPT/HT. Above this state, the statistical nature gradually appears in ESTPT/HT. Around the energy region of ν_2/σ_3 (or ν_3/σ_3) + $1\sigma_1$, the density of states changes from the order of 10^2 to 10^3 states/cm^{-1}. Therefore, the IVR rates may become similar (or larger) to the ESTPT/HT rates when the density of states exceeds the order of 10^3 states/cm^{-1}. Thus, the disappearance of the vibrational-mode specific nature of ESTPT/HT in the higher energy region ($\geq$600 cm^{-1}) has been successfully explained by the opening of the IVR process. The ESTPT/HT reaction has a statistical nature in the higher energy region. Thus, the nature of the mechanism of ESTPT/HT changes from vibrational-mode specific to statistical fashion with increasing the internal energy. To our best of knowledge, this is the first observation of changing the nature of the mechanism of the proton/hydrogen atom transfer reaction in aromatic molecules and molecular clusters.

D. Cooperative Phenomenon in ESTPT/HT. Figure 10 illustrates the hydrogen-bonded network in $7AI(CH_3OH)_2$ as directed graphs, where the directions of the hydrogen bonds are represented with the arrows.[75] In the directed graphs, the hydrogen-bonded network in $7AI(CH_3OH)_2$ is represented as one-dimensional hydrogen-bonded chains. In Figure 10 (b), the directions of all arrows in the normal form are reversed to those of the tautomeric form; i.e., the direction of the hydrogen-bonded network in the normal form is opposite to that of the tautomeric form. The ESTPT/HT is triggered by exciting the $\pi\pi^*$ state. Therefore, the photoexcitation that is limited to the electronic system in 7AI induces the reversion of the directions of *all* hydrogen bonds. In other words, the changes of the directions of the hydrogen bonds in $7AI(CH_3OH)_2$ simultaneously occur over the whole hydrogen-bonded network; hence, the terminology "simultaneously" does not mean the mechanism of ESTPT/HT but the static conformation after ESTPT/HT. This indicates that the direction of each hydrogen bond in $7AI(CH_3OH)_2$ cannot change independently; i.e., there are correlations in the directions of each hydrogen bond. These considerations show that ESTPT/HT in $7AI(CH_3OH)_2$ is a basic model system for the investigation of the cooperative phenomena about the reorganization of the hydrogen-bonded networks.

The reason why the cooperative ESTPT/HT occurs in $7AI(CH_3OH)_2$ is obvious. According to the ab initio calculations in ref 70, the energies of the configurations, where the hydrogen-bond directions are partially reversed, are too high to populate in our experimental conditions. Thus, the cooperative phenomenon in ESTPT/HT in $7AI(CH_3OH)_2$ is energetically driven. The investigation of the dynamics of the cooperative phenomenon in small systems is important to reveal the essential features of the cooperative phenomenon at the molecular level, which is quite difficult (or impossible) for the macroscopic systems due to the large numbers of degrees of freedom.

Conclusions

We have measured the mass-selected REMPI spectra of $7AI(CH_3OH)_2$-d_n ($n = 0-3$) and FE spectra obtained by detecting the UV and visible emission from the tautomeric form. Fluorescence from the tautomeric form was observed only from $7AI(CH_3OH)_2$. This shows the occurrence of the excited-state triple-proton and/or triple-hydrogen atom transfer (ESTPT/HT) in $7AI(CH_3OH)_2$. The nature of ESTPT/HT has been quantitatively characterized by introducing the acceleration factor (f_a). The comparison of the lower limit of the f_a values (f_a^{low}) of various vibronic states clearly show that ESTPT/HT is vibrational-mode specific in the low-energy region ($\Delta\nu\sim+600$ cm^{-1}). The excitation of the vibronic states containing the σ_1 mode remarkably accelerates ESTPT/HT, whereas the excitation of ν_2/σ_3 (or ν_3/σ_3) mode provides little effect on the ESTPT/HT rate. In contrast with the vibrational-mode specific behavior in the low-energy region, the behavior in the higher energy region is very different. The f_a^{low} values of $\nu_{intra}(744)$, $\nu_{intra}(744)$ + $1\sigma_1$, and $\nu_{intra}(1088)$ have been found to be similar. This drastic change of the behavior has been successfully explained by the statistical nature induced by IVR. The ESTPT/HT occurs from the vibrational energy redistributed states that contain the σ_1 mode. Thus, the nature of the mechanism of ESTPT/HT changes from vibrational-mode specific to statistical fashion with increasing the internal energy. To our best of knowledge, such internal-energy dependent change of the mechanism of the excited-state proton/hydrogen transfer reaction has been found for the first time.

We have shown that the directions of the hydrogen bond are completely reversed over the whole hydrogen-bonded network simultaneously after ESTPT/HT by representing the hydrogen-bonded network as the direct graphs. We suggest that ESTPT/HT in $7AI(CH_3OH)_2$ is a basic model system of the cooperative phenomenon, which is useful for the investigation of the dynamics of the cooperative phenomenon.

Acknowledgment. This work was supported in part by the Grant-in-Aid for Scientific Research No.15250015 and No. 18350013 from the Japanese Ministry of Education, Science, Sports and Technology.

Supporting Information Available: Details referring to Figure 3b,c. Figure S1 of REMPI spectra. Tables S1 and S2 of vibrational numbers. This material is available free of charge via the Internet at http://pubs.acs.org.

References and Notes

(1) In *Atom Tunneling Phenomena in Physics, Chemistry, and Biology*; Miyazaki, T. Ed.; Springer: Berlin, 2004.
(2) Zimmer, M. *Chem. Rev.* **2002**, *102*, 759.
(3) Lodish, H.; Berk, A.; Matsudaira, P.; Kaiser, C. A.; Krieger, M.; Scott, M. P.; Zipurski, L.; Darnell, J. *Molecular Cell Biology*; W. H. Freeman & Co., 2004.
(4) Kandori, H. *Biochim. Biophys. Acta* **2000**, *1460*, 176.
(5) Eikerling, M.; Kornyshev. A. A.; Kucernak, A. R. *Phys. Today* **2006**, *59*, 38.
(6) Pino, G. A.; Dedonder-Lardeux, C.; Gregoire, G.; Jouvet, C.; Martrenchard, S; Solgadi, D. *J. Chem. Phys.* **1999**, *111*, 10747.

(7) Pino, G. A.; Gregoire, G.; Dedonder-Lardeux, C.; Jouvet, C.; Martrenchard, S; Solgadi, D. *Phys. Chem. Chem. Phys*. **2000**, *2*, 893.
(8) Gregoire, G.; Dedonder-Lardeux, C.; Jouvet, C.; Martrenchard, S; Solgadi, D. *J. Phys. Chem. A* **2001**, *105*, 5971.
(9) Ishiuchi, S.; Saeki, M.; Sakai, M.; Fujii, M. *Chem. Phys. Lett.* **2000**, *322*, 27.
(10) Ishiuchi, S.; Daigoku, K.; Saeki, M.; Sakai, M.; Hashimoto, K.; Fujii, M. *J. Chem. Phys.* **2002**, *117*, 7077.
(11) Ishiuchi, S.; Daigoku, K.; Saeki, M.; Sakai, M.; Hashimoto, K.; Fujii, M. *J. Chem. Phys.* **2002**, *117*, 7083.
(12) Sobolewski, A. L.; Domcke, W.; Dedonder-Lardeux, C.; Jouvet, C. *Phys. Chem. Chem. Phys.* **2002**, *4*, 1093.
(13) Ashfold, M. N. R.; Cronin, B.; Devine, A. L.; Dixon, R. N.; Nix, M. G. D. *Science* **2006**, *312*, 1637.
(14) Gregoire, G.; Dedonder-Lardeux, C.; Jouvet, C.; Martrenchard, S.; Peremans, A.; Solgadi, D. *J. Phys. Chem. A* **2000**, *104*, 9087.
(15) Carrington, T.; Miller, W. H. *J. Chem. Phys.* **1986**, *84*, 4364.
(16) Shida, N.; Barbara, P. F.; Almlöf, J. E. *J. Chem. Phys.* **1989**, *91*, 4061.
(17) Shida, N.; Barbara, P. F.; Almlöf, J. E. *J. Chem. Phys.* **1991**, *94*, 3633.
(18) Sekiya, H.; Nagashima, Y.; Nishimura, Y. *J. Chem. Phys*. **1990**, *92*, 5761.
(19) Sekiya, H.; Nagashima, Y.; Tsuji, T.; Nishimura, Y.; Mori, A.; Takeshita, H. *J. Chem. Phys.* **1991**, *95*, 10311.
(20) Nishi, K.; Sekiya, H.; Kawakami, H.; Mori, A.; Nishimura, Y. *J. Chem. Phys.* **1999**, *111*, 3961.
(21) Taylor, C. A.; El-Bayoumi, M. A.; Kasha, M. *Proc. Natl. Acad. Sci. U.S.A.* **1969**, *63*, 253.
(22) Ingham, K. C.; Abu-Elgheit, M.; El-Bayoumi, M. A. *J. Am. Chem. Soc.* **1971**, *93*, 5023.
(23) Ingham, K. C.; El-Bayoumi, M. A. *J. Am. Chem. Soc.* **1974**, *96*, 1674.
(24) El-Bayoumi, M. A.; Avouris, P.; Ware, W. R. *J. Chem. Phys.* **1975**, *62*, 2499.
(25) Hetherrington, W. M., III; Micheels, R. H.; Eisenthal, K. B. *Chem. Phys. Lett.* **1979**, *66*, 230.
(26) Bulska, H.; Grabowski, A.; Pakula, B.; Sepiol, J.; Waluk, J.; Wild, U. P. *J. Lumin*. **1984**, *29*, 65.
(27) Tokumura, K.; Watanabe, Y.; Itoh, M. *Chem. Phys. Lett*. **1984**, *111*, 379.
(28) Tokumura, K.; Watanabe, Y.; Udagawa, M.; Itoh, M. *J. Am. Chem. Soc*. **1987**, *109*, 1346.
(29) Fuke, K.; Yoshiuchi, H.; Kaya, K. *J. Phys. Chem.* **1984**, *88*, 5840.
(30) Fuke, K.; Yabe, T.; Chiba, N.; Kohida, T.; Kaya, K.; *J. Phys. Chem.* **1986**, *90*, 2309.
(31) Fuke, K.; Kaya, K.; *J. Phys. Chem.* **1989**, *93*, 614.
(32) Fuke, K.; Tsukamoto, K.; Misaizu, F.; Kaya. K. *J. Chem. Phys.* **1991**, *95*, 4074.
(33) Share, P.; Pereira, M.; Sarisky, M.; Repinec, S.; Hochstrasser, R. M. *J. Lumin*. **1991**, *48/49*, 204.
(34) Chen, Y.; Rich, R. L.; Gai, F.; Petrich, J. W. *J. Phys. Chem*. **1993**, *97*, 1770.
(35) Douhal, A.; Kim, S. K.; Zewail, A. H. *Nature* **1995**, *378*, 260.
(36) Douhal, A.; Guallar, V.; Moreno, M.; Lluch, J. M. *Chem. Phys. Lett*. **1996**, *256*, 370.
(37) Nakajima, A.; Hirano, M.; Hasumi, R.; Kaya. K.; Watanabe, H.; Carter, C. C.; Williamson, J. M.; Miller, T. A. *J. Phys. Chem*. **1997**, *101*, 392.
(38) Lopez-Martens, R.; Long, P.; Sogaldi, D.; Soep, B.; Syage, J.; Millie, P. *Chem. Phys. Lett.* **1997**, *273*, 219.
(39) Takeuchi, S.; Tahara, T. *Chem. Phys. Lett*. **1997**, *277*, 340.
(40) Takeuchi, S.; Tahara, T. *J. Phys. Chem. A* **1998**, *102*, 7740.
(41) Takeuchi, S.; Tahara, T. *Chem. Phys. Lett*. **2001**, *347*, 108.
(42) Folmer, D. E.; Poth, L.; Wisniewski, E. S.; Castleman, A. W., Jr. *Chem. Phys. Lett.* **1998**, *287*, 1.
(43) Folmer, D. E.; Wisniewski, E. S.; Castleman, A. W., Jr. *Chem. Phys. Lett.* **2000**, *318*, 637.
(44) Chachisvilis, M.; Fiebig, T.; Douhal, A.; Zewail, A. H. *J. Phys. Chem. A* **1998**, *102*, 669.
(45) Fiebig, T.; Chachisvilis, M.; Manger, M.; Zewail, A. H.; Douhal, A.; Garcia-Ochoa, I.; de La Hoz Ayuso, A. *J. Phys. Chem. A* **1999**, *103*, 7419.
(46) Mente, S.; Maroncelli, M. *J. Phys. Chem. A* **1998**, *102*, 3860.
(47) Guallar, V.; Batista, V.; Miller, W. H. *J. Chem. Phys*. **1999**, *110*, 9922.
(48) Fiebig, T.; Chachisvilis, M.; Manger, M.; Zewail, A. H.; Douhal, A.; Garcia-Ochoa, I.; De la Hoz Ayuso, A. *J. Phys. Chem. A* **1999**, *103*, 7419.
(49) Sakota, K.; Hara, A.; Sekiya, H.; *Phys. Chem. Chem. Phys.* **2004**, *6*, 32.
(50) Hara, A.; Komoto, Y.; Sakota, K.; Miyoshi, R.; Inokuchi, Y.; Ohashi, K.; Kubo, K.; Yamamoto, E.; Mori, A.; Nishi, N.; Sekiya, H. *J. Phys. Chem. A* **2004**, *108*, 10789.
(51) Sakota, K.; Sekiya, H. *J. Phys. Chem. A* **2005**, *109*, 2718.
(52) Sakota, K.; Sekiya, H. *J. Phys. Chem. A* **2005**, *109*, 2722.
(53) Sakota, K.; Okabe, C.; Nishi, N.; Sekiya, H. *J. Phys. Chem. A* **2005**, *109*, 5245.
(54) Komoto, Y.; Sakota, K.; Sekiya, H. *Chem. Phys. Lett.* **2005**, *406*, 15.
(55) Sekiya, H.; Sakota, K. *Bull. Chem. Soc. Jpn.* **2006**, *79*, 373.
(56) Catalan, J.; Kasha, M. *J. Phys. Chem. A* **2000**, *104*, 10812.
(57) Catalan, J.; Perez, P.; del Valle, J. C.; de Paz, J. L. G.; Kasha, M. *Proc. Natl. Acad. Sci. U.S.A.* **2004**, *101*, 419.
(58) Matsumoto, Y.; Ebata, T.; Mikami, N. *J. Phys. Chem. A* **2002**, *106*, 5591.
(59) Tanner, C.; Manca, C.; Leutwyler, S. *Science* **2003**, *302*, 1736.
(60) Manca, C.; Tanner, C.; Coussan. S.; Leutwyler, S. *J. Chem. Phys.* **2004**, *121*, 2578.
(61) Tanner, C.; Manca, C.; Leutwyler, S. *J. Chem. Phys.* **2005**, *122*, 204326.
(62) Manca, C.; Tanner, C.; Leutwyler, S. *Int. Rev. Phys. Chem.* **2005**, *24*, 457.
(63) Tanner, C.; Thut, M.; Steinlin, A.; Leutwyler, S. *J. Phys. Chem. A* **2006**, *110*, 1758.
(64) McMorrow, D.; Aartsma, T. *Chem. Phys. Lett.* **1986**, *125*, 581.
(65) Moog, R. S.; Bovino, S. C.; Simon, J. D. *J. Phys. Chem.* **1988**, *92*, 6545.
(66) Chapman, C. F.; Maroncelli, M. *J. Phys. Chem.* **1992**, *96*, 8430.
(67) Moog, R. S.; Maroncelli, M. *J. Phys. Chem.* **1991**, *95*, 10359.
(68) Mente, S.; Maroncelli, M. *J. Phys. Chem. A* **1998**, *102*, 3860.
(69) Kwon, O.−H.; Lee, Y.-S.; Park, H. J.; Kim, Y. K.; Jang, D.-J. *Angew. Chem., Int. Ed.* **2004**, *43*, 5792.
(70) Sakota, K.; Komoto, Y.; Nakagaki, M.; Ishikawa, W.; Sekiya, H. *Chem. Phys. Lett.* **2007**, *435*, 1.
(71) Yokoyama, H.; Watanabe, H.; Omi, T.; Ishiuchi, S.; Fujii, M. *J. Phys. Chem. A* **2001**, *105*, 9366.
(72) Huang, Y.; Arnold, S.; Sulkes, M. *J. Phys. Chem.* **1996**, *100*, 4734.
(73) Yamada, Y.; Katsumoto, K.; Ebata, T. *Phys. Chem. Chem. Phys.* **2007**, *9*, 1170.
(74) Stein, S. E.; Rabinovitch, B. S. *J. Chem. Phys.* **1973**, *58*, 2438.
(75) Miyake, T.; Aida, M. *Chem. Phys. Lett.* **2002**, *363*, 106.